Proceedings IRF2018: 6th International Conference Integrity-Reliability-Failure
Lisbon/Portugal 22-26 July 2018. Editors J.F. Silva Gomes and S.A. Meguid
Publ. INEGI/FEUP (2018); ISBN: 978-989-20-8313-1

PAPER REF: 7185

DISCRETE ELEMENTS SIMULATION OF GEOLOGICAL FAULT FORMATION

Vadim Lisitsa[1(*)], Vladimir Tcheverda[1], Victoria Valyanskaya[2]
[1]Institute of Petroleum Geology and Geophysics SB RAS, Novosibirsk, Russia
[2]OAO "Rosneft", Moscow, Russia
[(*)]*Email:* Lisitsavv@ipgg.sbras.ru

ABSTRACT

In this work, we implement discrete element method for simulation of fault zone formation due to the tectonic deformations of the Earth crust. Discrete element simulation provides us with the valuable information on the deformations distribution in the vicinity of the fault, which can be recomputed into the petrophysical parameters of the core. The final model is the spatial distribution of the densities and seismic waves velocities which are used for seismic modelling.

Keywords: discrete element method, fault formation, seismic modelling.

INTRODUCTION

Simulation of finite deformations in solids and, in particular, in the geomaterials, geostructures, core samples and Earth crust can be done by either grid-based methods such as finite differences [Erickson *et al*., 2001], [González *et al*., 2008], finite elements [Guiton *et al*., 2003], boundary elements [Resor, Pollard, 2012] or by meshless approaches also known as discrete elements method (DEM) [Gray *et al*., 2014], [Lisjak, Grasselli, 2014]. The letter is preferred because no predefined crack or fault geometry is needed for simulation. However, particle-based methods are more computationally intense and require calibration of the particle properties to match the mechanics of the whole body [Lisjak, Grasselli, 2014], [Alassi, Holt, 2012]. In spite of this the particle-based methods are extremely flexible and can be used to generate multiple statistical realizations of the fault zones and study statistical features of the strongly deformed and highly-distorted zones. This opens a possibility to analyze the correlations between the peculiarities in the fault structure and their responses to the seismic waves. Moreover, use of the graphical processor units (GPU) significantly reduces the computational time making the DEM simulations an efficient and flexible tool.

In this paper, we present the approach to simulate fault formation in inhomogeneous media based on the discrete element modelling implemented on the GPU. In the first section, we provide an overview of the approach, describe the particles contact model, and remind the time integration finite-difference scheme. Next, we describe the numerical experiments to simulate large deformations and fault formation in homogeneous and horizontally layered media. After that, we will use the finite deformations to estimate the elastic properties of the fault zone to construct the set of models for further seismic modelling [Vishnevsky *et al*., 2017], [Kolyukhin *et al*., 2017; Kostin *et al*., 2015].

DISCRETE ELEMENTS FOR SOLIDS

In this section, we formulate the basic principles of the discrete elements used for the simulation of the finite deformations in geological formations. At the scale of the tectonic deformations, we can restrict the considerations with the linear model of particle interactions. Moreover, we neglect the rotation of the elements, and consider only the static and dynamic friction due to sliding [Botter *et al*., 2014], [Hardy, Finch, 2005], [Hardy, Finch, 2007], [Hardy *et al*., 2009].

Consider two particles numbered i and j (Figure 1). Denote coordinates of their centers by $\vec{x}^i$ and $\vec{x}^j$ respectively and their radii R^i and R^j. Vector $\vec{X}_{ji} = \vec{x}^i - \vec{x}^j$ is directed from the center of j-th element to the center of i-th element, and vector $\vec{h}_{ji} = \vec{X}_{ji} / \left\| \vec{X}_{ji} \right\|$ is the unit vector directed correspondingly. In these notations, elastic interaction between the two particles (the normal force) can be defined as (Figure 1a):

$$\vec{F}_{ji}^{n} = \begin{cases} K_r^- \left(R_i + R_j - \left\| \vec{X}_{ji} \right\| \right) \vec{n}_{ji}, & R_i + R_j - \left\| \vec{X}_{ji} \right\| > 0, \quad repulsion \\ K_r^+ \left(R_i + R_j - \left\| \vec{X}_{ji} \right\| \right) \vec{n}_{ji}, & 0 < \left\| \vec{X}_{ji} \right\| - R_i - R_j < r_0, \quad active\_bond \\ 0 & \left\| \vec{X}_{ji} \right\| - R_i - R_j > r_0 \quad no\_bond \end{cases} \quad (1)$$

Constants and are the elastic modulae, defining the intensity of the repulsion and attraction. In general these two modulae and be completely different [Lisjak, Grasselli, 2014], [Luding, 2008], however, for the geomaterials they typically coincide [Hardy *et al*., 2009]. Note, that is a limiting distance between two particles, so that if the distance between the particles exceeds the limit, the bond breakage accuses. This allows simulation of the cracks and faults formation.

According to the numerical study conducted by several independent researches [Abe et al., 2011], [Cundall, Strack, 1979], [Duan *et al*., 2017], [Gray *et al*., 2014], [Hardy *et al*., 2009], [O'Sullivan *et al*., 2003] macroscopic properties of the materials are mainly depend on the model of friction at the microscopic level, rather than elastic interaction. A classical model of friction is based on the Coulomb law, where two types of friction are considered. The first one is the friction of rest, which is defined by the relative displacement of the particles and is independent on their velocity. However, if the friction of the rest exceeds a particular value, the relative motion starts dominating, and the friction is defined by the relative velocities of the particles. Formally, the tangential forces due to the friction can be represented as

$$\vec{F}_{ji}^{s} = \begin{cases} K_t \delta_t \vec{t}^{ji} & K_t \delta_t \le \mu^s \left\| \vec{F}_{ji}^{n} \right\| \\ -\mu^d \left\| \vec{F}_{ji}^{n} \right\| sign\left(\vec{v}^{ji}, \vec{t}^{ji} \right) \vec{t}^{ji} & K_t \delta_t > \mu^s \left\| \vec{F}_{ji}^{n} \right\| \end{cases} \quad (2)$$

where $\vec{t}^{ji}$ is the unitary tangential vector, i.e. $(\vec{t}^{ji}, \vec{h}^{ji}) = 0$. Vector $\vec{v}^{ji} = \vec{v}^i - \vec{v}^j = \frac{d\vec{x}^i}{dt} - \frac{d\vec{x}^j}{dt}$ is the relative velocity vector. Parameter K_t is a shear modulus, which is typically close to the elastic modulus K_r^+, δ_t is the relative displacement for the rest position, and $\mu^d < \mu^s$ are the dynamic and static friction coefficients. A sketch of the tangential forces appeared between two interacting particles are presented in Figure 1b.

In order to make the system stable at large enough time of simulation an artificial dissipation is used

$$\vec{F}_i^d = -\nu \frac{d\vec{x}^i}{dt} \quad (3),$$

where is the dissipation parameter. The particular choice of this parameter is discussed in [Luding, 2008].

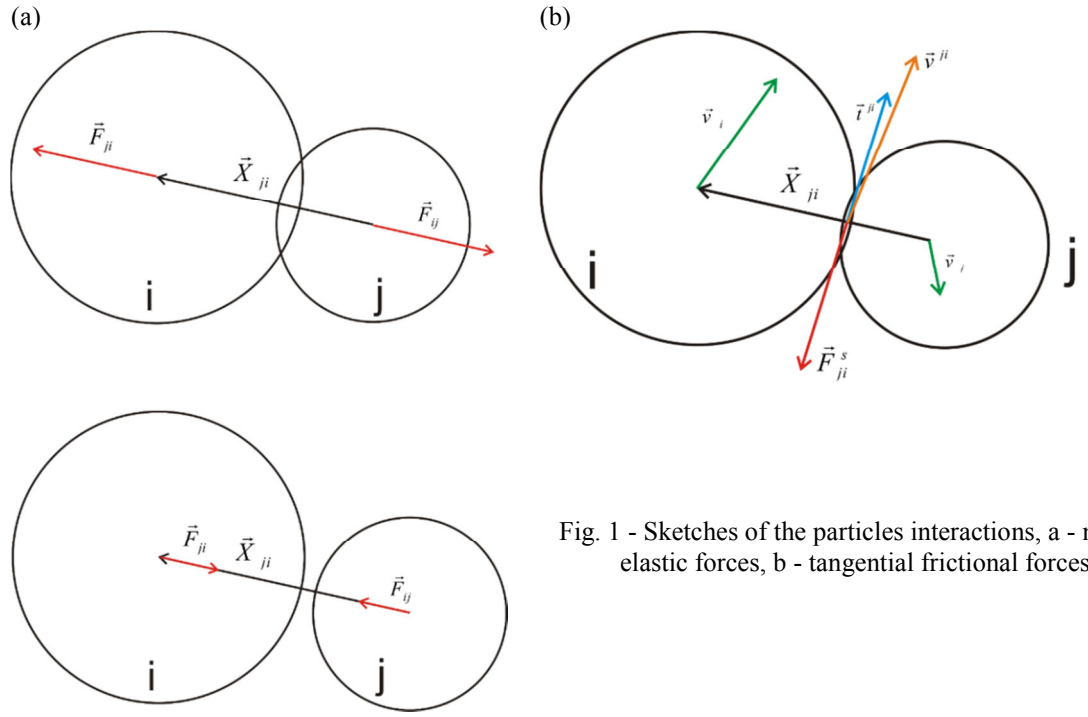

Fig. 1 - Sketches of the particles interactions, a - normal elastic forces, b - tangential frictional forces.

INTEGRATION OF THE EQUATIONS OF MOTION

Having defined all the forces acting at the particles, due to elastic interaction, friction, artificial dissipation, and, possibly external forces we can write down the equations of motion, following the Newtonian mechanics:

$$M^j \frac{d^2\vec{x}^j}{dt^2} = \sum_{i \in J(i)} \left(\vec{F}_{ji}^n(\vec{x}^i, \vec{x}^j) + \vec{F}_{ji}^t(\vec{x}^i, \vec{x}^j) \right) - \nu \frac{d\vec{x}^j}{dt} \quad (4)$$

In case of pure elastic interaction, the normal forces do not depend on the particle velocity, whereas the explicit dependence is governed by the dissipative term. In contrary to the DEM simulation of gas and fluid dynamics, where friction and dissipation may be neglected, in the considered case presence of the frictional forces reduces the order of approximation of widely used Verlet scheme. Note also that, the interaction between the particles is local, thus very limited number of neighbors affect the particular particle (let us say i-th particle). This leads

to the stencil-like simulations, strictly reducing the number of floating-point operations. In particular one may estimate the maximal number of the neighbors:

$$\dim(J(i)) \le \frac{2\pi}{arctg\left(\frac{2R_m}{R_M + R_m + r_0}\right)},$$

where R_M and R_m are the maximal and minimal radii of the particles in the system, and r_0 is the bond length. Typically $r_0 \le 0.05R_m$, thus it can be neglected. For our further simulations we will use the radii distribution so that $R_m \approx 0.5R_M$, thus the maximal number of the neighbors will be $\dim(J(i)) \le 11$. In case of small deformations one may assume that the bonds are fixed and never brake up, thus the neighbors are also fixed and the discrete element method is equivalent to the finite differences or finite volumes. [Hu *et al*., 2017], [Wang *et al*., 2017].

Following [Hardy, Finch, 2005], [Hardy, Finch, 2007], [Mora, Place, 1994] we use the Verlet scheme:

$$\begin{aligned} &\frac{(\vec{x}^j)^{n+1} - (\vec{x}^j)^n}{\tau} = (\vec{v}^j)^n + \frac{\tau}{2}\left(\vec{F}^j\right)^n / M^j, \\ &\frac{(\vec{v}^j)^{n+1} - (\vec{v}^j)^n}{\tau} = 0.5\left(\left(\vec{F}^j\right)^{n+1} + \left(\vec{F}^j\right)^n\right) / M^j \end{aligned} \qquad (5)$$

where $(\vec{x}^j)^n$ is the coordinate of the j-th particle at instant $t = n\tau$, τ is the time step, $(\vec{v}^j)^n$ is the velocity of the j-th particle at instant $t = n\tau$, and $(\vec{F}^j)^n$ is the force acting at the j-th particle at the same instant. If the forces are smooth enough functions of their arguments and there is no dissipation, when scheme (5) approximates equations of motion (4) with the second order. However, if friction and dissipation is included into the system, when the order of approximation decreases down to the first.

NUMERICAL EXPERIMENTS

The first series of the numerical experiments was done to simulate fault forming in a homogeneous media. We consider different values of the internal dynamic friction coefficient and study its effect on the fault formation. To make the simulations consistent with previously published results we consider the particle's properties the same as in the paper [Botter *et al*., 2014]; i.e. Bulk modulus of particles $K_r = 7.8GPa$, bond length $r_0 = 0.05R_m$, dissipation coefficient $\nu = 100$ kg/s, shear modulus $K_s = K_r$, static friction coefficient $\mu^s = 0.8$, dynamic friction coefficient μ^d varies. The size of the domain is 2000 by 500 m. Diameters of the elements varied from 1.25 to 2.5 m using uniform distribution. We simulate 60° dipping normal fault, with vertical displacement equal to 100 m. We provide several stages of the fault formation for dynamic friction coefficient $\mu^d = 0.3$ (figure 2) and $\mu^d = 0.1$ (figure 3). We present the relative deformations in the fault zone and also introduce coloring of artificial layers (original model is homogeneous) to illustrate the displacements. According to the presented results, formation of the fault takes place along particular inclined planes. The smaller the dynamic friction the flatter the fault is.

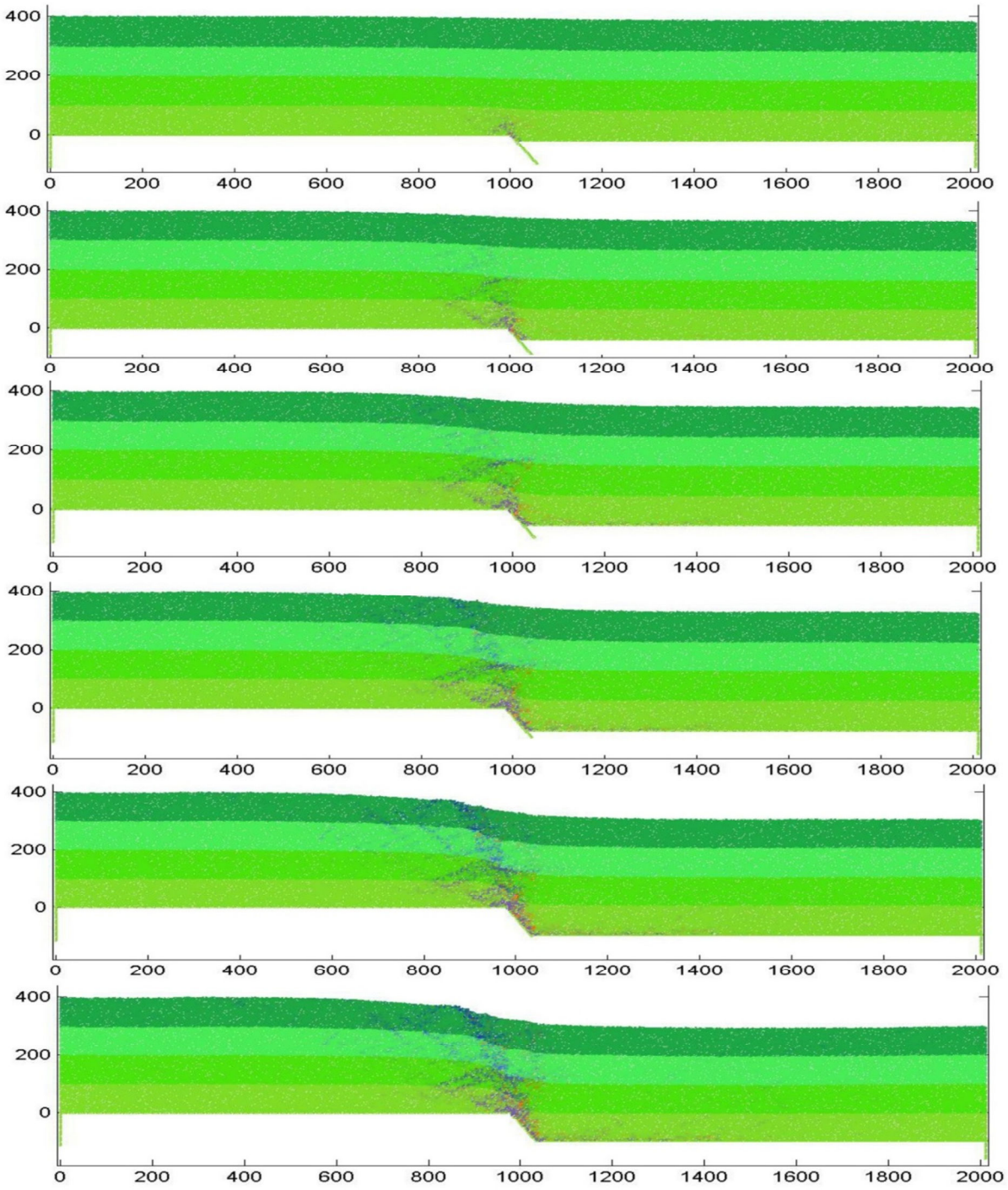

Fig. 2 - Relative volumetric strains for the model with $\mu^d = 0.3$, for vertical displacements 15, 30, 45, 60, 75, and 90 meters.

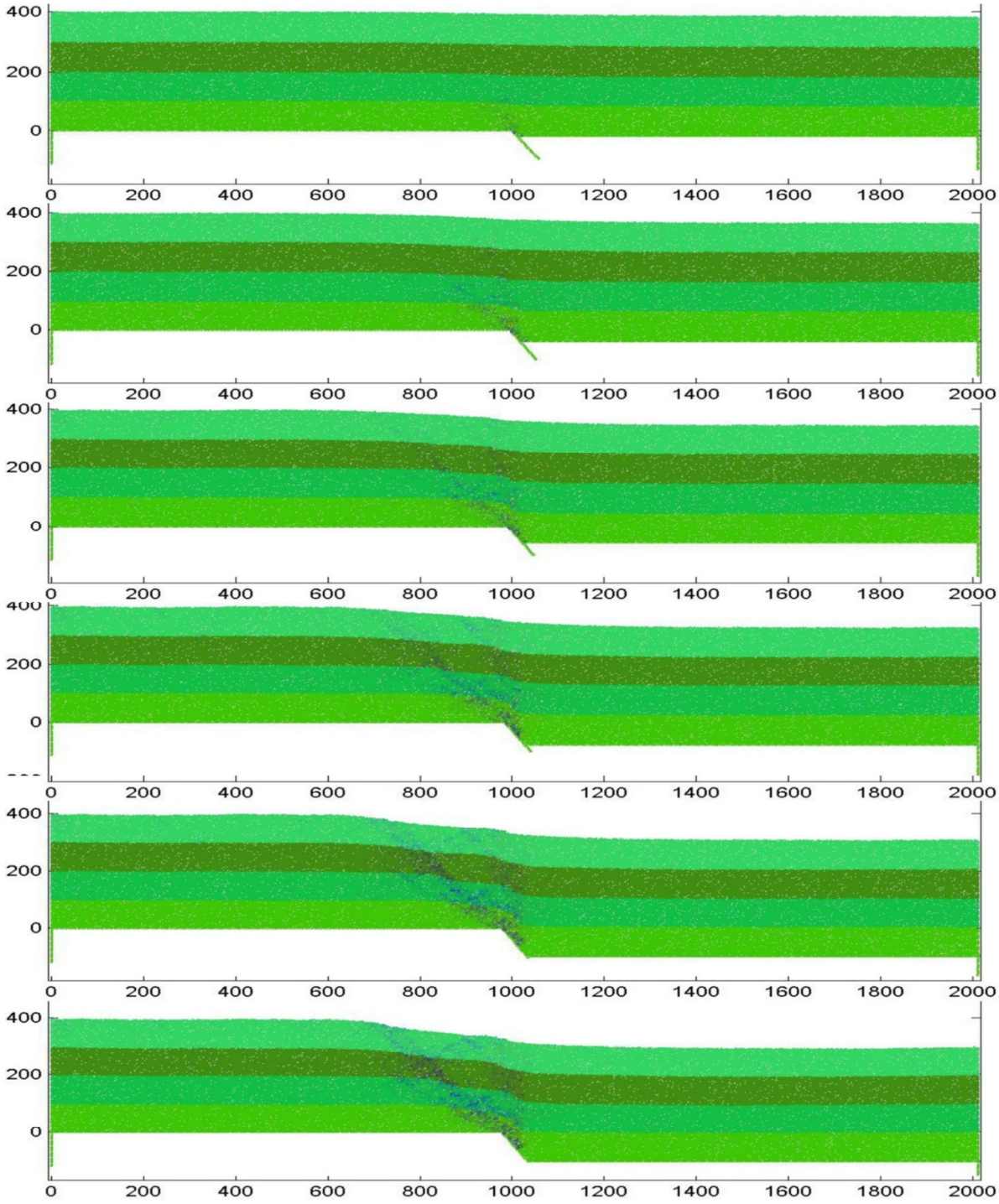

Fig. 3 - Relative volumetric strains for the model with $\mu^d = 0.1$, for vertical displacements 15, 30, 45, 60, 75, and 90 meters.

The second set of experiments is done for a layered media, where shale layers are alternating by the layers of sandstone. Following [Botter *et al*., 2014] we consider the physical properties of the particles representing shale and sandstone coinciding and being equal to those used in the previous experiment. The different is modeled by using dynamic friction coefficients equal to 0.3 for sandstone and 0.1 for shale. Having computed the finite deformations for the layered model we use the empirical relations between the strains and elastic modules of the

rocks to estimate seismic velocities in the vicinity of the faults [Holt *et al*., 2008], [Skurtveit *et al*., 2013], [Hatchell, Bourne, 2005]. In particular, we consider quadratic relations for the longitudinal wave speed:

$$V_P = \begin{cases} V_P^0(-0.25\varepsilon^2 - 0.5\varepsilon + 1), & -1 \le \varepsilon < 0 \\ V_P^0(0.25\varepsilon^2 - 0.5\varepsilon + 1), & 0 \le \varepsilon \le 1 \end{cases}$$

where V^0 is the reference velocity in unperturbed model, ε is the relative volumetric strain. The shear wave velocity is estimated as $V_s = V_p / \sqrt{3}$. Results (estimated velocities) for several statistical realizations are presented in figure 4, where the formed fault zone presents causing local decrease of the wave propagation velocities.

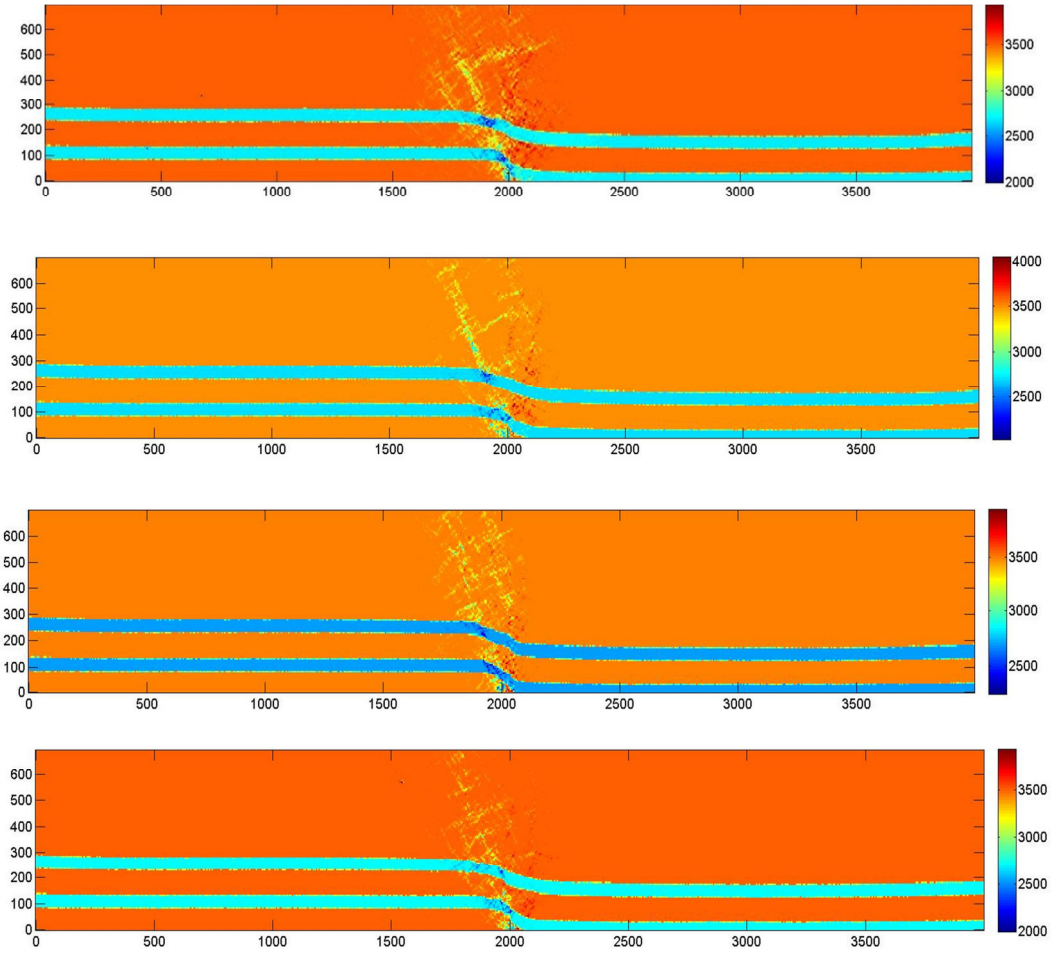

Fig. 4 - Examples of the P-wave velocity estimation in the fault zone by discrete element modelling.

CONCLUSIONS

We presented an approach for numerical simulation of the fault formation process, based on the discrete element method. This approach allows reconstructing the fault zone which is the result of finite deformations in the rock formaition. In contrary to the grid-based methods,

discrete elements do not require predetermined fault position. Moreover, size of the particles can be changed and typically statistically distributed. This makes the DEM simulations attractive from the geostatistical point of view, because allows simulating multiple statistical realizations of the fault zones.

We estimate the seismic parameters in the fault zone on the base of the empirical relations, however, we admit that to be more accurate and close to the reality we need to use DEM at the core scale to simulate fraturing or formation of the deformation bonds in the core samples. After that we can follow the evolution of the elastic properties of the core under increaseing finite deformations.

ACKNOWLEDGMENTS

The research was done under financial support of Russian Science Foundation grant no. 17-17-01128. Numerical simulations were performed on cluster NKS-30T of the Siberian Supercomputer Center.

REFERENCES

[1] Abe S., Gent H. V., and Urai J. L. DEM simulation of normal faults in cohesive materials // Tectonophysics. 2011. V. 512. pp. 12-21.

[2] Alassi H. T., and Holt R. Relating discrete element method parameters to rock properties using classical and micropolar elasticity theories // International Journal for Numerical and Analytical Methods in Geomechanics. 2012. V. 36. N. 10. - pp. 1350-1367.

[3] Botter C. *et al*., From mechanical modeling to seismic imaging of faults: A synthetic workflow to study the impact of faults on seismic // Marine and Petroleum Geology. 2014. V. 57. pp. 187-207.

[4] Cundall P. A., and Strack O. D. L. A discrete numerical model for granular assemblies // Géotechnique. 1979. V. 29. N. 1. pp. 47-65.

[5] Duan K., Kwok C. Y., and Ma X. DEM simulations of sandstone under true triaxial compressive tests // Acta Geotechnica. 2017. V. 12. N. 3. pp. 495-510.

[6] Erickson S. G., Strayer L. M., and Suppe J. Initiation and reactivation of faults during movement over a thrust-fault ramp: numerical mechanical models // Journal of Structural Geology. 2001. V. 23. N. 1. pp. 11-23.

[7] González G., et al. Crack formation on top of propagating reverse faults of the Chuculay Fault System, northern Chile: Insights from field data and numerical modelling // Journal of Structural Geology. 2008. V. 30. N. 6. pp. 791-808.

[8] Gray G. G., Morgan J. K., and Sanz P. F. Overview of continuum and particle dynamics methods for mechanical modeling of contractional geologic structures // Journal of Structural Geology. 2014. V. 59. N. Supplement C. pp. 19-36.

[9] Guiton M. L. E., *et al*. Mechanical constraints on the chronology of fracture activation in folded Devonian sandstone of the western Moroccan Anti-Atlas // Journal of Structural Geology. 2003. V. 25. N. 8. pp. 1317-1330.

[10] Hardy S., and Finch E. Discrete-element modelling of detachment folding // Basin Research. 2005. V. 17. N. 4. pp. 507-520.

[11] Hardy S., and Finch E. Mechanical stratigraphy and the transition from trishear to kink-band fault-propagation fold forms above blind basement thrust faults: A discrete-element study // Marine and Petroleum Geology. 2007. V. 24. pp. 75-90.

[12] Hardy S., McClayc K., and Munozb J. A. Deformation and fault activity in space and time in high-resolution numerical models of doubly vergent thrust wedges // Marine and Petroleum Geology. 2009. V. 26. pp. 232-248.

[13] Hatchell P., and Bourne S. Rocks under strain: Strain-induced time-lapse time shifts are observed for depleting reservoirs // The Leading Edge. 2005. V. 24. N. 12. pp. 1222-1225.

[14] Holt R.M., *et al*. (2008), Strain Sensitivity of Wave Velocities in Sediments and Sedimentary Rocks, edited, American Rock Mechanics Association.

[15] Hu X., Jia X., and Zhang W. (2017), An arbitrary order dynamic lattice method for elastic wave modeling in TTI media, in SEG Technical Program Expanded Abstracts 2017, edited, pp. 4225-4230.

[16] Kolyukhin D. R., et al. Seismic imaging and statistical analysis of fault facies models // Interpretation. 2017. V.5. N. 4. pp. SP71-SP82.

[17] Kostin V., et al. Local time-space mesh refinement for simulation of elastic wave propagation in multi-scale media // Journal of Computational Physics. 2015. V. 281. N. 0. pp. 669-689.

[18] Lisjak A., and Grasselli G. A review of discrete modeling techniques for fracturing processes in discontinuous rock masses // Journal of Rock Mechanics and Geotechnical Engineering. 2014. V. 6. N. 4. pp. 301-314.

[19] Luding S. Introduction to discrete element methods // European Journal of Environmental and Civil Engineering. 2008. V. 12. N. 7-8. pp. 785-826.

[20] Mora P., and Place D. Simulation of the frictional stick-slip instability // Pure and Applied Geophysics. 1994. V. 143. N. 1. pp. 61-87.

[21] O'Sullivan C., D. Bray J., and Li S., A new approach for calculating strain for particulate media // International Journal for Numerical and Analytical Methods in Geomechanics. 2003. V. 27. N. 10. pp. 859-877.

[22] Resor P. G., and Pollard D.D., Reverse drag revisited: Why footwall deformation may be the key to inferring listric fault geometry // Journal of Structural Geology. 2012. V. 41. pp. 98-109.

[23] Skurtveit E., *et al*., Experimental investigation of deformation mechanisms during shear-enhanced compaction in poorly lithified sandstone and sand // Journal of Geophysical Research: Solid Earth. 2013. V. 118. N. 8. pp. 4083-4100.

[24] Vishnevsky D. M., *et al*., Correlation analysis of statistical facies fault models // Dokl. Earth Sc. 2017. V. 473. N. 2. pp. 477-481.

[25] Wang S., *et al*. (2017), Viscoacoustic wave simulation by lattice Boltzmann method and the relationship between relaxation factor and the quality factor, in SEG Technical Program Expanded Abstracts 2017, edited, pp. 4102-4106.